Acta metall. mater. Vol. 38, No. 11, pp. 2175–2185, 1990
Printed in Great Britain. All rights reserved

0956-7151/90 $3.00 + 0.00
Copyright © 1990 Pergamon Press plc

THEORY OF ELECTRON-IRRADIATION-INDUCED AMORPHIZATION

A. T. MOTTA† and D. R. OLANDER

University of California at Berkeley, CA 94720 and Materials and Chemical Sciences Division, Lawrence Berkeley Laboratory, Calif., U.S.A.

(*Received* 17 *July* 1989; *in revised form* 11 *April* 1990)

Abstract—The crystalline–amorphous transformation of the intermetallic precipitates $Zr_2(Fe, Ni)$ and $Zr(Cr, Fe)_2$ in Zircaloy under irradiation is studied. Experiments show that the dose-to-amorphization increases exponentially with temperature and decreases with dose rate. A model for the transformation is proposed that accounts for these observations. In this model amorphization is caused by the destabilization of the crystalline phase with respect to the amorphous phase caused by an irradiation-induced increase in its free energy. Contributions to the free energy increase due to both point defect increases and irradiation-induced-disordering are calculated and found to have approximately the same magnitude. The disordering contribution is independent of temperature and dose rate, since thermal reordering is small compared to ballistic disordering for the temperatures of interest. The temperature and dose rate dependences of the dose-to-amorphization are given by the point defect contribution. This indicates that electron-irradiation-induced amorphization is caused not only by irradiation-induced disordering but also by an increase in point defect concentration. A simplified version of the model valid at high temperature finds that the controlling parameter for amorphization is the parameter $\text{dpa}.k^{1/2}$, where dpa is the dose and k the dose rate. This model is then compared with other models in the literature on the basis of amorphization kinetics and of the temperature and dose rate dependence of the dose-to-amorphization. The characteristics of the amorphous transformation under electron irradiation and neutron irradiation are discussed. It is believed that different amorphization mechanisms are operative in each case.

Résumé—La transformation cristal–amorphe sous irradiation électronique des précipités intermetalliques $Zr(Cr, Fe)_2$ et $Zr_2(Ni, Fe)$ dans le Zircaloy est étudiée. Les résultats expérimentaux montrent que la dose pour amorphiser augmente exponentiellement avec la température et décroît avec le taux d'endommagement. Un modèle est proposé pour expliquer ces résultats. Selon ce modèle, l'amorphisation est causée par une déstabilisation de la phase cristalline irradiée par rapport à la phase amorphe, due a une augmentation de L'énergie libre lors de l'irradiation. Les contributions à la croissance de l'énergie libre apportées par l'augmentation de la concentration des défauts ponctuels et par le désordre chimique sont calculées, leurs contributions étant trouvées comparables. La contribution due au désordre chimique est indépendante de la température et du taux d'endommagement, la mise en ordre thermique étant trop faible par rapport au désordre ballistique dans le domaine de température étudié. La variation de la dose nécessaire à l'amorphisation avec la température ainsi qu'avec le taux d'endommagement est donnée par l'acroissement du nombre de défauts ponctuels. Cela indique que les deux phénomènes, désordre chimique et augmentation de la concentration des défauts ponctuels, sont tous les deux nécessaires à l'amorphisation sous irradiation électronique. Dans une version simplifiée du modèle, valable à haute température, l'amorphisation est contrôlée par le paramètre $\text{dpa} \cdot k^{1/2}$, où dpa est la dose et k le taux d'endommagement. Le modèle est comparé avec d'autres modèles de la littérature, du point de vue de la cinétique de l'amorphisation, et de la dépendance de la dose nécessaire à l'amorphisation vis à vis de la température et du taux d'endommagement. Les caractéristiques de la transformation amorphe sous irradiation neutronique et électronique sont aussi comparées. Il semble que, dans les deux cas, l'amorphisation soit provoquée par des mécanismes différentes.

Zusammenfassung—Die bestrahlungsinduzierte kristallin–amorphe Umwandlung der intermetallischen Ausscheidungen $Zr_2(Fe, Ni)$ und $Zr(Cr, Fe)_2$ wird untersucht. Die Experimente zeigen, daß die Amorphisierungsdosis exponentiell mit der Temperatur zunimmt und mit der Dosisrate abnimmt. Ein diese Beobachtungen berücksichtigendes Modell wird für diese Umwandlung vorgeschlagen. Hierin tritt Amorphisierung dadurch auf, daß die freie Energie der kristallinen Phase bestrahlungsinduziert erhöht und dadurch die amorphe Phase begünstigt wird. Die Beiträge zu dieser Erhöhung der freien Energie durch Punktfehler und durch die bestrahlungsinduzierte Entordnung werden berechnet; sie sind vergleichbar. Der Entordnungsbeitrag ist unabhängig von Temperatur und Dosisrate, da die thermische Ordnungseinstellung im Vergleich zur ballistischen Entordnung im betrachteten Temperaturbereich klein ist. Die Punktfehlerverteilung bestimmt die Tempertur- und Dosisratenabhängigkeit der Amorphisierungsdosis.

†Present address: CENG/SECC, 85x, 38041 Grenoble, France.

Das bedeutet, daß die durch Elektronenbestrahlung induzierte Amorphisierung nicht nur durch die bestrahlungsinduzierte Entordnung, sondern auch durch einen Anstieg in der Punktfehlerkonzentration verursacht wird. Aus einer vereinfachten Version des Modells für hohe Temperaturen geht hervor, daß der bestimmende Parameter für die Amorphisierung $\mathrm{dpa} \cdot k^{1/2}$ ist; hierbei sind dpa die Dosis und k die Dosisrate. Das Modell wird mit anderen Modellen der Literatur im Hinblick auf die Amorphisierungskinetik und der Temperatur- und Dosisratenabhängigkeit der Amorphisierungsdosis verglichen. Die Eigenheiten der amorphen Umwandlung unter Elektronen- und Neutronenbestrahlung werden diskutiert. Es sieht so aus, als ob in diesen Fällen unterschiedliche Amorphisierungsmechanismen vorliegen.

1. INTRODUCTION

The zirconium-based alloy Zircaloy is extensively used as fuel cladding and fuel assembly material in light water reactors because of its good mechanical, thermal and nuclear properties. The nuclear industry is presently exploring the possibility of increasing the residence time of fuel elements in the reactor, which raises the possibility that the favorable microstructural characteristics of the alloy might be altered under prolonged irradiation with concomitant degradation of its mechanical properties.

The standard as-fabricated microstructure of Zircaloy contains the intermetallic precipitates $Zr(Cr, Fe)_2$ and $Zr_2(Ni, Fe)$ in a zirconium matrix. The precipitate morphology is an important factor in determining the strength, ductility and corrosion resistance of the alloy. Recently [1, 2], precipitates have been observed to undergo a crystalline–amorphous transformation (amorphization) under neutron irradiation. The transformation was found to be temperature-dependent and more likely to occur at lower temperatures. To study this effect on an accelerated time scale, a means is needed of delivering radiation damage much more rapidly than neutron irradiation. Electron irradiation is well suited to this purpose because it provides temperature control and damaging irradiation with simultaneous observation of the damage.

Several studies on the electron-irradiation-induced amorphization of various intermetallic compounds have recently been published [3–11]. The theoretical models advanced in those studies explain amorphization as being caused by a destabilization of the irradiated crystalline phase with respect to the amorphous phase due to an increase in its free energy under irradiation. Such irradiation-induced free energy increase can be stored in the material in the form of increased chemical disorder [6], or in the form of a higher concentration of point defects [7–10]. Here chemical disorder means an increase in the number of like pairs of atoms at the expense of the energetically-favored unlike-pair configurations.

Through the experiments made by Luzzi *et al.* [11] and the observation that intermetallic solid solutions do not amorphize under electron irradiation [6], chemical disordering has been clearly linked to amorphization of intermetallic compounds. The role of point defects has not been as clearly established, chiefly because the attainability of high enough point defect concentrations in the face of elimination by recombination has not been demonstrated [12].

In a recent paper, we proposed a model that explains amorphization under electron irradiation utlizing both point defect accumulation and chemical disordering [13]. It is the purpose of this article to establish that a model of electron-irradiation-induced amorphization needs to include point defect increase in order to explain the temperature and dose rate dependence of the dose-to-amorphization.

2. EXPERIMENT

2.1. Experimental methods

Thin foils for transmission electron microscopy were prepared from Zircaloy-2 rods furnished by Teledyne Wah-Chang of Albany, Oregon, using standard electropolishing techniques as explained in [14].

Specimens were irradiated in the microscope until the intermetallic precipitate under observation became amorphous. The electron beam was produced in the Kratos 1.5 MeV HVEM at the National Center of Electron Microscopy at Lawrence Berkeley Laboratory. The dose in displacements per atom (dpa) and the dose rate (dpa/s) were measured. The measured dose was corrected for the Gaussian shape of the beam, and beam heating was taken into account by performing a heat transfer calculation for a simplified foil geometry [14]. The temperature corrections obtained were of the order of 10 K which agrees well with the literature [15, 16]. Specimen temperatures ranged from 110 to 310 K when corrected for that effect.

Diffraction patterns were taken at regular intervals to ascertain the occurrence of amorphization. The intensity of the diffracted peaks (normalized to the intensity of the transmitted beam) defines the degree of crystallinity ψ

$$\psi = \frac{\left(\frac{I_{\mathrm{diff}}}{I_{\mathrm{trans}}}\right) \text{at } t = t_{\mathrm{irr}}}{\left(\frac{I_{\mathrm{diff}}}{I_{\mathrm{trans}}}\right) \text{at } t = 0}. \tag{1}$$

The quantity ψ is unity at the start of the experiment and zero when the specimen becomes amorphous (i.e. the spot pattern disappears and a ring pattern emerges).

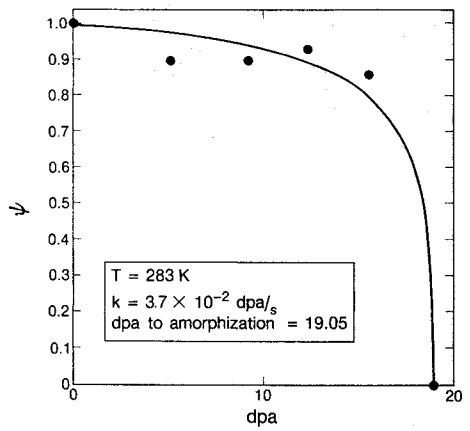

Fig. 1. Degree of crystallinity ψ vs irradiation dose (dpa).

The irradiated precipitates were further examined for composition variations (solute segregation, precipitate dissolution) in a Philips EM400 with an EDX attachment.

2.2. *Experimental results*

Figure 1 shows an example of the evolution of ψ: it remains close to 1 throughout the irradiation, decreasing sharply at the end. This behavior suggests that amorphization occurs relatively quickly throughout the entire precipitate near the end of the irradiation time. This implies that the kinetics of amorphization are fast, compared to the irradiation time, and that the thermodynamic driving force controls the observed behavior.

In some larger precipitates amorphization was observed to occur first in the center, then to slowly spread outward. A typical amorphization series is shown in Fig. 2(a). The amorphous spot was always found to be located at the center of the condensed electron beam [Fig. 2(b)] rather than at the center of the precipitate itself. This is evidence that the matrix had little influence on the amorphization process. Further confirmation of this was obtained by irradiating bulk Zr_2Ni (prepared by arc melting). The dose-to-amorphization of the bulk specimens was found to be the same as that of precipitates in Zircaloy. Good agreement was also found with the results from irradiation of bulk Zr_2Ni [17]. This result supports the conclusion that, unlike under neutron [18] and ion [19] irradiation, the amorphization of precipitates in Zircaloy under electron irradiation occurs without participation of the matrix.

The growth of the amorphous area is plotted against irradiation time in Fig. 2(c). The shape of this curve is roughly Gaussian, suggesting that amorphization at the center of the beam was due to the larger dose delivered here. This explains the small (10%) variation in ψ before complete amorphization (Fig. 1).

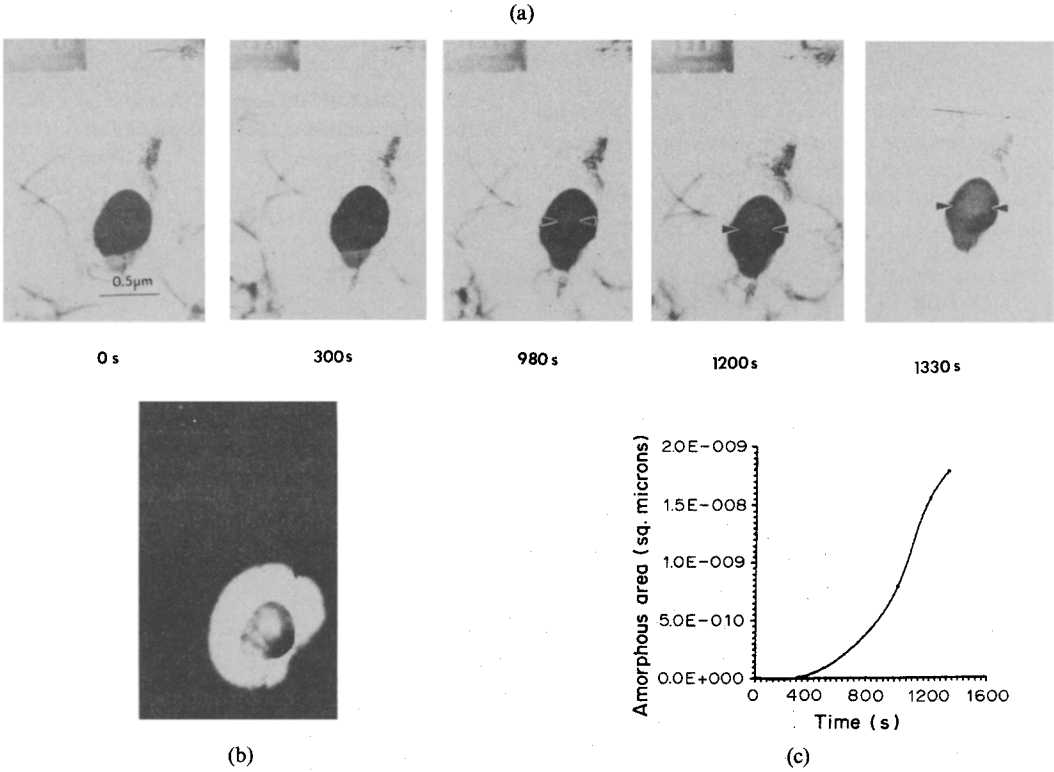

Fig. 2. (a) Bright field series of amorphization experiment of Zr_2(Ni, Fe) ($T = 272$ K, $k = 9 \times 10^{-3}$ dpa/s). The diameter of the amorphous region (indicated by the arrows) increases with irradiation time. (b) Bright field of the condensed electron during irradiation. (c) Amorphous spot area vs irradiation time for the experiment above.

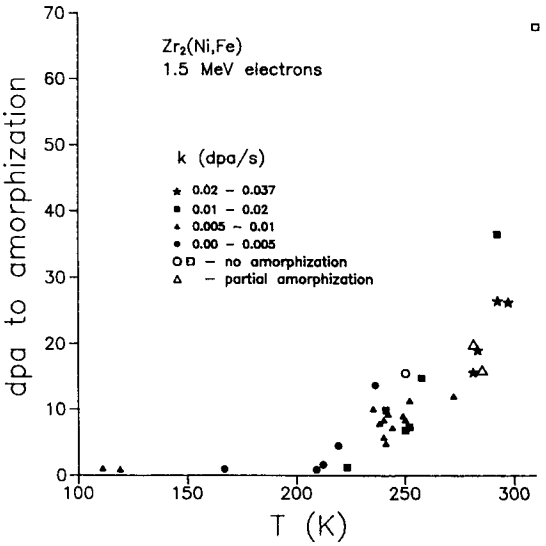

Fig. 3. Dose-to-amorphization vs temperature for Zr_2(Ni, Fe) precipitates. Four dose rate ranges are shown.

The dose-to-amorphization for Zr_2(Ni, Fe) precipitates is shown in Fig. 3. It increases exponentially with temperature as found previously [3, 15]. Above ≈ 300 K, no amorphization could be detected even for very high doses. Dose rates have been grouped in four different ranges for easier visibility of the dose rate effect on the dose-to-amorphization. As can be seen in Fig. 3, the dose-to-amorphization was found to be lower for higher dose rates. The results for Zr(Cr, $Fe)_2$ precipitates are shown later in Fig. 6.

The precipitate dissolution and iron depletion that were observed in neutron irradiation [20, 21] were not present in this study. Precipitate compositions were the same before and after amorphization.

3. THEORETICAL MODEL OF AMORPHIZATION UNDER ELECTRON IRRADIATION

The amorphization condition is:

$$\Delta G_{irr} \geqslant \Delta G_{ac} \tag{2}$$

where ΔG_{ac} is the difference in free energy between the amorphous and unirradiated crystalline states and ΔG_{irr} is the difference between the free energy of the irradiated and unirradiated crystals. The irradiation-induced free energy change is subdivided in two parts

$$\Delta G_{irr} = \Delta G_{def} + \Delta G_{dis}. \tag{3}$$

ΔG_{def} is the increase in free energy due to the point defect concentration increase and ΔG_{dis} is the contribution due to chemical disordering. The sum of those two contributions, as calculated by the model described in the following sections, is then compared to the experimental value of ΔG_{ca} obtained from the literature [13, 14, 22, 23].

3.1. Free energy change due to point defect accumulation

The change in free energy due to point defect accumulation is

$$\Delta G_{def} = \Delta H_{def} - T_{irr}\Delta S_{def} = \sum_{j=i,v} C_j \Omega_j - RT_{irr} \sum_{j=i,v} [C_j \ln C_j + (1 - C_j)\ln(1 - C_j)] \tag{4}$$

where C_j is the concentration of point defect species j and Ω_j is the energy associated with its formation. The subscripts i and v stand for interstitial and vacancy, respectively.

To find the concentrations of point defects as functions of time, the transient point defects balances must be solved. This was done for the case of a thin foil (approximated by a flat slab) subject to a spatially-uniform displacement rate due to the electron flux, with recombination and taking into account the diffusion to free surfaces [13].

The relevant equations are

$$\frac{\partial C_v}{\partial t} = D_v \frac{\partial^2 C_v}{\partial x^2} + k - K_{iv} C_i C_v$$

$$\frac{\partial C_i}{\partial t} = D_i \frac{\partial^2 C_i}{\partial x^2} + k - K_{iv} C_i C_v \tag{5}$$

with the boundary conditions $C_i = C_v = 0$ at $x = L$ and $\partial C_v/\partial x = \partial C_i/\partial x = 0$ at $x = 0$ for all t. The initial condition is $C_i = C_v = 0$ at $t = 0$ for all x. Here K_{iv} is the recombination coefficient, k is the dose rate (dpa/s), D_i and D_v are the interstitial and vacancy diffusion coefficients, x is the spatial variable perpendicular to the foil surface, and L is the half thickness of the foil. Equation (5) can be written in non-dimensional form

$$\Gamma \frac{\partial y_v}{\partial \tau} = \epsilon \frac{\partial^2 y_v}{\partial \chi^2} + 1 - y_i y_v$$

$$\frac{1}{\Gamma} \frac{\partial y_i}{\partial \tau} = \epsilon \frac{\partial^2 y_i}{\partial \chi^2} + 1 - y_i y_v \tag{6}$$

where the non-dimensional variables are defined as follows

$$y_v = \sqrt{\frac{D_v}{D_i}}\Theta_v \quad y_i = \sqrt{\frac{D_i}{D_v}}\Theta_i$$

$$\Theta_v = \sqrt{\frac{K_{iv}}{k}} C_v \quad \Theta_i = \sqrt{\frac{K_{iv}}{k}} C_i \quad \chi = \frac{x}{L}$$

$$\tau = \sqrt{K_{iv} k}\, t \quad \epsilon = \frac{\sqrt{D_i D_v}}{L^2 \sqrt{K_{iv} k}} \quad \Gamma = \sqrt{\frac{D_i}{D_v}}. \tag{7}$$

The use of two non-dimensional point defect concentrations is for clarity in presenting the results. The system of equations (6) was solved numerically [13, 14]. The results indicate that:

(1) The interstitial concentrations are much smaller than the vacancy concentrations because the

more mobile interstitials are eliminated at the surface while the vacancies remain in the lattice.

(2) The concentration of vacancies does not vary much from the midplane to the surface of the foil (at most a factor of 2)

(3) The steady-state condition ($D_i C_i = D_v C_v$) is not reached for the irradiation conditions of interest.

(4) After a brief startup period where $\Theta_i = \Theta_v = kt$, and during the long approach to steady state, the numerical solution can be approximated analytically by

$$\Theta_v = 3.9\,\tau^{1/2} \tag{8}$$

$$\Theta_i = 25\,\tau^{-1/2}. \tag{9}$$

The period during which the approximations above are valid comprises most of the irradiation time for any choice of parameters as long as $D_i/D_v > 10^5$ so equations (8) and (9) are taken to represent point defect behavior thoughout the experiment. This period is equivalent to the recombination-dominated, low temperature, period found in rate theory [24], which also shows a square root dependence on dose.

Converting to dimensional variables

$$C_v = 3.9\left(\frac{k}{K_{iv}}\right)^{1/4}\sqrt{kt} \tag{10}$$

$$C_i = 25\left(\frac{k}{K_{iv}}\right)^{1/4}\frac{1}{\sqrt{kt}}. \tag{11}$$

Another study [25] performed the same numerical calculation in the approach to steady state for a thin foil subject to electron irradiation, finding the same results as in [13]. However, a fortuitous combination of parameters that made $\tau \approx t$ ($\sqrt{K_{iv}k} \approx 1$) hid the dose rate dependence of the point defect concentrations.

Equation (10) shows that C_v has, in addition to the square root dependence on the fluence, a one-fourth power dependence on the dose rate k and the recombination coefficient K_{iv}. For high dose rates, the precipitates amorphize more quickly, since C_v is higher for a given fluence, compared to a low dose rate case. Since K_{iv} is dependent on temperature through the diffusion coefficient. C_v drops exponentially with increasing temperature, and therefore causes the dose-to-amorphization to rise exponentially, as observed experimentally.

Since the interstitial concentration is much smaller than the vacancy concentration, it is neglected in equation (4). The increase in free energy due to the addition of point defects is then

$$\Delta G_{def} = C_v \Omega_v R\,T_{irr}\,[C_v \ln C_v + (1 - C_v)\ln(1 - C_v)] \tag{12}$$

with C_v given by equation (10).

3.2. *Free energy change due to disordering*

As shown above, the temperature and dose rate dependence of the dose-to-amorphization are explained by the different point defect concentrations attained under different irradiation conditions.

However, since $Zr_2(Ni, Fe)$ is an ordered alloy, it is subject to disordering under irradiation. We evaluate here the disordering contribution to the free energy increase with the object of showing that it is of the same order of magnitude as the contribution due to point defect increase. The disordering kinetics are also calculated to compare the relative values of the irradiation disordering and thermal reordering terms.

The free energy change due to disordering is given by

$$\Delta G_{dis} = \Delta H_{dis} - T_{irr}\Delta S_{dis} = NV\Delta C_{ab} - RT_{irr}\sum_{i=a,b}\sum_{j=a,b} F_{ij}\ln F_{ij} \tag{13}$$

where ΔC_{ab} is the change in the number of A–B bonds per lattice site, N is the total number of lattice sites per mol, V is the ordering energy and the F_{ij} are the probabilities of finding an i-type atom on a j-type site. Ideally, C_{ab} should be given by the short-range order parameter, which is a direct measure of the number of A–B bonds present in the material. In this study the Bragg–Williams approximation will be used [26], in which there is no short-range order above what would be expected from the presence of long-range order as defined by the long-range-order parameter $\mathbf{S}$

$$\mathbf{S} = \frac{F_{aa} - x_a}{1 - x_a} = \frac{F_{bb} - x_b}{1 - x_b} \tag{14}$$

where x_a and x_b are the atomic fractions of atoms type A and B. With the approximation above, C_{ab} is

$$C_{ab} = A_2\mathbf{S}^2 + A_1\mathbf{S} + A_0 \tag{15}$$

where A_0, A_1 and A_2 are constants that depend on the crystal structure and stoichiometry of the alloy. For $Zr_2(Ni, Fe)$, $A_0 = 16/9$, $A_1 = 2/9$ and $A_2 = 2/3$ [14]. ΔC_{ab} is then the change in the number of A–B pairs as the long-range order parameter changes from 1 to $\mathbf{S}$

$$\Delta C_{ab} = C_{ab}(1) - C_{ab}(\mathbf{S}) = A_2(1 - \mathbf{S}^2) + A_1(1 - \mathbf{S}) \tag{16}$$

$\mathbf{S}$ is reduced by irradiation disordering and increased by thermal reordering.

The irradiation disordering process considered in this study is random recombination [27]. In random recombination, some of the atoms displaced from their lattice sites return to the lattice by recombining with vacancies. As the point defect formation energy is approximately one order of magnitude larger than the ordering energy, recombination is essentially random.

Since care was taken to insure that the beam direction did not coincide with exact orientations of close-packed rows of lattice atoms, and since secondary displacements are very few for electron

irradiation, disordering by replacement collision sequences [28] is not included in the model. The change in S due to random recombination is given by [27, 29]

$$\left(\frac{dS}{dt}\right)_{RR} = -kS. \tag{17}$$

Two thermal reordering mechanisms are considered in the appendix: a vacancy and a split-interstitial mechanism. For the irradiation conditions in this study, the vacancy mechanism is shown to be much smaller than the disordering term, while the split-interstitial mechanism is found to be potentially able to offset random recombination. There are indications, however, that Fe and Ni are fast diffusers in Zr [30], diffusing through a direct interstitial mechanism. This has been explained on the basis of the atomic size difference between Zr and (Fe,Ni). This means that atomic exchanges between the Zr and (Fe, Ni) sublattices will not be favored in the alloy. Therefore, even if interstitial migration in the alloy occurs by a split-interstitial mechanism, it is likely to occur through the individual Zr and (Fe, Ni) sublattices, thereby not affecting the degree of order. The split-interstitial reordering mechanism is therefore neglected in the present analysis.

Neglecting reordering, S can be written as

$$S(t) = S_0 e^{-kt}. \tag{18}$$

To calculate ΔG_{dis}, equation (13) is used where ΔC_{ab} given by equation (16) with S from equation (18). The F_{ij} can be found as a function of S using equation (14) and the conservation of lattice sites neglecting occupation by point defects ($F_{ba} + F_{aa} = F_{ab} + F_{bb} = 1$) [13].

3.3. *Total free energy change and condition for amorphization*

From equations (12) and (13), the total free energy change given by equation (3) is

$$\begin{aligned}\Delta G_{irr} = {} & C_v\Omega_v - RT_{irr}[C_v \ln C_v + (1 - C_v)\ln(1 - C_v)] \\ & + NV[A_2(1 - S^2) + A_1(1 - S)] \\ & - RT_{irr} \sum_{i=a,b} \sum_{j=a,b} F_{ij} \ln F_{ij}\end{aligned} \tag{19}$$

with C_v given by equation (10) and S by equation (18).

The parameters used in the calculation are summarized in Table 1. E_i and D_{io} were used as fitting parameters. One example of the results of a full ΔG_{irr} calculation is shown in Fig. 4. The contributions due

Table 1. Zr_2(Ni, Fe) calculation parameters for finding ΔG_{def} and ΔG_{dis}

Ω_i	interstitial formation energy	4 eV
Ω_v	vacancy formation energy	1 eV
E_i	interstitial migration energy	0.4 eV
$\frac{D_v}{D_i}$	diffusion coefficient ratio	$< 10^{-5}$
V_0	ordering energy	0.025 eV
K_{iv0}	recombination coefficient	3×10^{16} (cm^{-2})
D_{io}	interstitial diffusion pre-exponential factor	10 (cm^2/s)

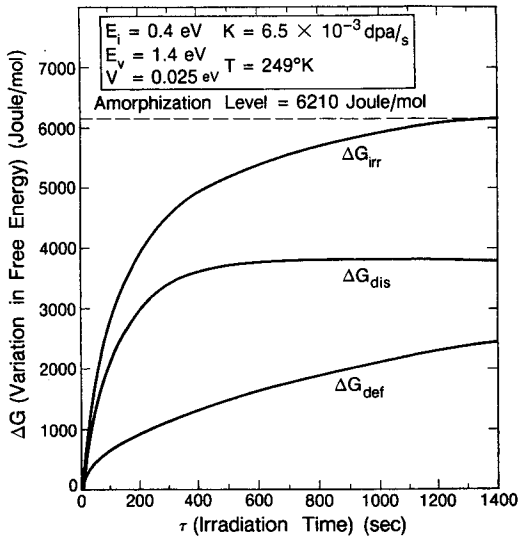

Fig. 4. Total free energy increase ΔG_{irr} for a Zr_2(Ni, Fe) precipitate as a function of irradiation time for the irradiation conditions indicated. The two free energy components, ΔG_{dis} due to disordering and ΔG_{def} due to point defect concentration increase, are also shown, as well as the Zr_2Ni amorphization level [22, 23].

to the buildup of point defects and radiation-induced disordering are seen to be equally important. In this case ΔG_{dis} rises sharply and subsequently levels off as S approaches zero. The precipitate disorders completely before amorphizing, as assumed in [5]. The disordering kinetics as calculated by the model are independent of temperature while the kinetics of point defect increase are slower at high temperatures due to increased annealing. Therefore at high temperatures the irradiation time necessary for a large ΔG_{def} to develop allows ΔG_{dis} to reach saturation long before amorphization occurs. At lower temperatures amorphization is reached more quickly and without full disordering through a larger contribution of ΔG_{def}. As a consequence of this behavior, a simplified version of the model applicable to high-temperature irradiation can be obtained. Rearranging equation (10)

$$\text{dpa} = kt = \left(\frac{C_v}{3.9}\right)^2 \left(\frac{K_{iv}}{k}\right)^{1/2}. \tag{20}$$

At amorphization, then

$$\text{dpa}_{final} k^{1/2} = A\,(C_{vfinal}^2)\, e^{-E_i/2k_BT} \tag{21}$$

where $A = (K_{iv0}D_{io})^{1/2}/3.9^2$ is a constant and K_{iv0} is the pre-exponential in the recombination coefficient. From equation (4)

$$C_v = \frac{\Delta H_{def}}{\Omega_v} \approx \frac{\Delta G_{def}}{\Omega_v} = \frac{\Delta G_{irr} - \Delta G_{dis}}{\Omega_v}. \tag{22}$$

Since $T\Delta S_{def} \approx 0.1\,\Delta H_{def}$, it is neglected in equation (22). From equation (2), at amorphization

$$C_{vfinal} \approx \frac{\Delta G_{ca} - \Delta G_{dis}}{\Omega_v} = \text{constant}. \tag{23}$$

Since disordering occurs rapidly compared to point defect accumulation, as seen in Fig. 4, the ΔG_{dis} contribution to the free energy increase under irradiation is constant and corresponds to the change in free energy as S goes from 1 to 0. This means that for all temperatures at which complete disordering occurs before amorphization ΔG_{def} and C_{vfinal} have a fixed value at amorphization. Taking $T\Delta S_{def} = 0.1\Delta H_{def}$, the calculated C_{vfinal} is 0.009. So we can write

$$\text{dpa}_{final} k^{1/2} = Be^{-E_i/2k_B T} \tag{24}$$

where $B = A(C_{vfinal})^2$ is a constant. For the present assumptions, then the quantity dpa.$k^{1/2}$ is an effective unit of damage for amorphization under electron irradiation [13, 14]. This quantity is dependent only on temperature since the dose rate dependence was factored in. It is interesting to note that the same effective unit of damage was reported for ion-implantation-induced amorphization of silicon [31].

Equation (24) can be plotted in Arrhenius fashion for both Zr_2(Ni, Fe) and Zr(Cr, $Fe)_2$, since the analysis above is also valid for the Cr-rich precipitates. This is shown in Figs 5 and 6. The doses-to-amorphization are comparable for Zr_2(Ni, Fe) and Zr(Cr, $Fe)_2$, with the latter being slightly easier to amorphize than the former. It can be seen that equation(24) is valid only for the high temperature points. The data scatter for Zr(Cr, $Fe)_2$ is considerably larger than for Zr_2(Ni, Fe). This could be due to the larger difference in diffusion coefficients between Fe and Cr than between Fe and Ni. Fluctuations in the Fe/Cr ratio would thus have more effect on the average diffusion coefficient in the precipitate, and consequently on the dose-to-amorphization, then would fluctuations in the Fe/Ni ratio.

The least squares approximation for the high temperature points gives for Zr_2(Ni, Fe) $E_i = 0.45$ eV and $D_{io} = 4\,\text{cm}^2/\text{s}$, which is in good agreement with the values of Table 1 used in the full calculation of ΔG_{irr}.

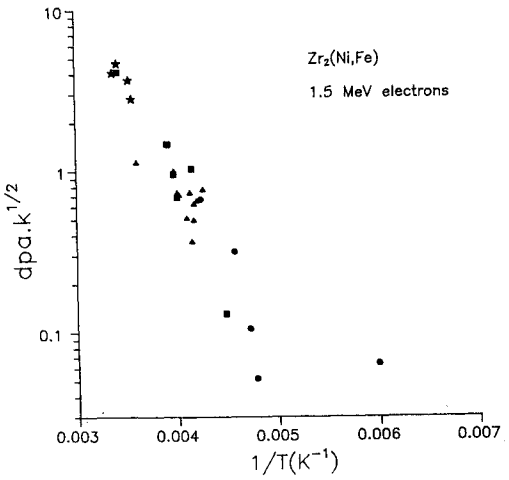

Fig. 5. Arrhenius plot of dpa.$k^{1/2}$ for Zr_2(Ni, Fe). The dose rate symbols are the same as in Fig. 3.

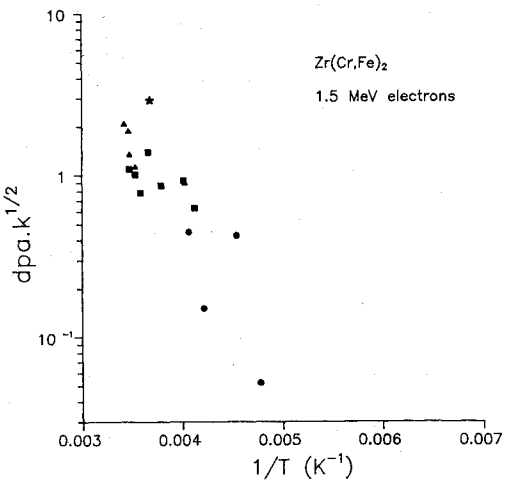

Fig. 6. Arrhenius plot of dpa.$k^{1/2}$ for Zr(Cr, $Fe)_2$. The dose rate symbols are the same as in Fig. 3.

The values of 0.40 eV and $10^{-2}\text{cm}^2/\text{s}$ were obtained for E_i and D_{io} in Zr(Cr, $Fe)_2$ using ΔG_{ca} from Ref. [32].

4. DISCUSSION

In this section two mechanisms of free energy storage in the irradiated lattice, point defect increase and chemical disorder, are discussed in light of the experimental results.

4.1. Point defect increase

The concept of a critical defect concentration above which the material becomes amorphous was first advanced by Swanson and co-workers [33], who estimated that a defect concentration between 0.02 and 0.04 site fraction is required to cause amorphization. Thomas *et al.* [3] also assume that amorphization is caused by an increase in the concentration of point defects and cite the amorphization resistance of thin regions in the foil as evidence, arguing that the presence of free surfaces depresses the concentration of point defects. Limoge and Barbu [7] emphasize the role of interstitials in the amorphization process, since large concentrations of vacancies can be absorbed in the lattice of some compounds by departures from stoichiometry. In addition, the amorphization process is clearly related to the motion of a point defect at a temperature where vacancies are thought to be immobile.

The above models do not include mechanisms for large increases in the concentration of point defects in the face of the kinetic limitation imposed by point defect recombination. In addition, the temperature dependence of the dose to amorphization is not considered.

These problems were addressed by other workers. Simonen [8] used rate theory to model the amorphiza-

tion kinetics of NiTi under electron irradiation. It was found that an interstitial migration energy of the order of 1 eV was necessary to rationalize the observed kinetics. This value is higher than most estimates of interstitial migration energies in metals. Pedraza and Mansur [5, 9, 10] postulated the existence of vacancy–interstitial complexes that are stabilized by a chemically favorable local environment. They calculated the amorphization kinetics in Zr_3Al due to the evolution of the complexes finding good agreement with experiment for a complex binding energy of 0.7–1 eV. Therefore, this mechanism is restricted to alloys where such complexes exist and have high binding energies. This condition might not apply to all intermetallics that amorphize under electron irradiation.

The model proposed in this work presents a viable mechanism for the point defect increase to the levels required for amorphization, while avoiding the difficulty of a recombination limit by allowing the accumulation of only one kind of point defect.

4.2. Chemical disorder

A clear link between chemical disordering and amorphization under electron irradiation was established by Luzzi *et al.* [11]. They measured the minimum degree of order (S_{min}) attainable under electron irradiation as a function of temperature and found a large increase in S_{min} between 275 and 300 K. At 275 K S_{min} is approximately 0.3, while at 300 K S_{min} is close to 1.0. This temperature range is coincident with the T_c for amorphization in the intermetallic compounds they studied (Cu_4Ti_3 and CuTi).

Based on the above experiments, Luzzi *et al.*. [11] propose that chemical disorder is both necessary and sufficient to cause amorphization. There are, however, two problems with this conclusion. First, the behavior of S_{min} (Fig. 7, Ref. [11]) shows that at 260 K the degree of order remained constant between 2 and 3.3 dpa, when amorphization occurred. Since S was constant, there was no increase in free energy due to chemical disorder between 2 and 3.3 dpa, and therefore some other mechanism of free energy increase must have been in operation. Such a mechanism could be an increase in free energy due to point defects, as shown in Fig. 4, where ΔG_{dis} reaches saturation but the continued increase in ΔG_{def} finally causes amorphization. Second, it is not apparent how the reduction of the dose-to-amorphization for higher dose rates observed in the present study could be explained by the pure chemical disordering model.

Furthermore, while no metallic solid solutions have been observed to amorphize under electron irradiation [6], some intermetallic compounds disorder without amorphizing [3, 7]. Therefore, it is proposed that disordering is a necessary but not sufficient condition for amorphization. It is necessary to supplement it with the increase in point defect concentration in order to explain the temperature and dose rate dependence of the dose-to-amorphization.

In the same reference, Luzzi *et al.* also propose a vacancy reordering mechanism to explain the temperature dependence of the dose-to-amorphization. From their experimental results such a mechanism would have to operate at 300 K but not at 260 K. The results of Banerjee and Urban [27] and Liou and Wilkes [34], which predict a sharp transition in the degree of order at the temperature of vacancy migration, are cited as evidence for a vacancy reordering mechanism. The critical temperature in these studies, however, was of the order of 600 K, which makes them inapplicable to the present case. Calculations of the vacancy reordering term (Appendix and also in Refs [35–37]) show it to be much smaller than the random recombination disordering term for the temperatures of interest (≈ 300 K).

On the other hand, since Cu and Ti have a smaller size ratio than Zr and (Fe, Ni), it is possible that the split-interstitial migration occurs with sublattice exchange in the Cu–Ti compounds. If that is the case, split-interstitial reordering could offset random recombination disordering at ≈ 265 K and no disordering would occur at higher temperatures. This could explain the reduced disordering observed above 265 K in Cu_4Ti_3 [11].

4.3. Comparision with neutron-irradiation-induced amorphization

The characteristics of neutron-irradiation-induced amorphization are similar in some respects to electron-irradiation-induced amorphization, but quite different in others. Both processes are dependent on fluence: a damage level of 1–10 dpa must be reached before amorphization occurs. Also, in both cases amorphization is more likely to occur at lower temperatures and there is a critical temperature above which amorphization does not occur for any fluence. There are some fundamental differences, however:

1. The critical temperature for amorphization is approximately 250 K higher for neutrons than for electrons.

2. Under neutron irradiation amorphization has been observed [1, 2, 18, 21] to start at the precipitate-matrix interface and advance inwards. Precipitates exhibited a crystalline core and an amorphous periphery. The amorphous zone was depleted in iron by about 30%. This suggests that the precipitate-matrix interface plays a role in the amorphization process, perhaps through an influx of point defects from the matrix. The electron-irradiation-induced process, in contrast, was seen (Section 2) to be essentially independent of the matrix. In addition, no compositional variation was observed.

5. CONCLUSIONS

1. The dose-to-amorphization under electron irradiation increases exponentially with temperature

and is smaller for higher dose rate. The dose-to-amorphization for $Zr(Cr, Fe)_2$ precipitates is similar to that for $Zr_2(Ni, Fe)$ precipitates in Zircaloy.

2. The kinetics of the crystalline-amorphous transformation under electron irradiation are fast compared to the irradiation time.

3. A theoretical model of electron-irradiation-induced amorphization is proposed that includes the contributions of point defect concentration increase and disordering. Both contributions are found to be equivalent. The temperature and dose rate dependence of the dose to amorphization are explained by the model.

4. Thermal reordering cannot account for the temperature dependence of the dose-to-amorphization because vacancy reordering is too small at the temperatures of interest and split-interstitial reordering is thought not to occur for the intermetallics in this study. It also cannot account for the observed dose rate dependence of the dose-to-amorphization.

5. Electron-irradiation-induced amorphization is found to be qualitatively different from neutron-irradiation-induced amorphization. Different amorphization mechanisms appear to be operative in each.

6. The significant role played by the surface sink in the point defect balances indicates that the utmost care is needed in the simulation of the effects of neutron irradiation with electron irradiation. Surface effects are an inherent part of electron irradiation of thin foils but are not present in bulk irradiation.

Acknowledgements—The assistance of the staff at the NCEM at LBL in doing the electron irradiations is deeply appreciated. This work was partially sponsored by EPRI under contract number RP-1250-14 and supported in part by the Director, Office of Energy Research, Office of Basic Energy Science, Materials Science Division of the U.S. Department of Energy under Contract Number DE-AC03-76SF00098. The financial support received from the Brazilian National Research Council (CNPq) by one of us (ATM) is gratefully acknowledged.

REFERENCES

1. W. J. S. Yang, R. P. Tucker, B. Cheng and R. B. Adamson, *J. Nucl. Mater.* **138,** 185 (1986).
2. M. Griffiths, R. W. Gilbert and G. J. C. Carpenter, *J. Nucl. Mater.* **150,** 53 (1987).
3. G. Thomas, H. Mori, H. Fujita and R. Sinclair, *Scripta metall.* **16,** 589 (1982).
4. H. Mori and H. Fujita, *Int. Symp. on In Situ Experiments with HVEM, Osaka Univ. Japan*, pp. 465–471 (1985).
5. D. Pedraza, *Radiat. Effects Defects Solids* **112,** 11 (1990).
6. D. E. Luzzi and M. Meshii, *Res. Mechanica* **21,** 207 (1987).
7. Y. Limoge and A. Barbu, *Phys. Rev. B* **30,** 2212 (1984).
8. E. P. Simonen, *Nucl. Instrum. Meth. Phys. Res.* **B16,** 198 (1986).
9. D. F. Pedraza, *J. Mater. Res.* **1,** 425 (1986).
10. D. F. Pedraza and L. K. Mansur, *Nucl. Instrum. Meth. Phys. Res.* **B16,** 203 (1986).
11. D. E. Luzzi, H. Mori, H. Fujita and M. Meshii, *Acta metall.* **34,** 629 (1986).
12. R. W. Cahn and W. L. Johnson, *J. Mater. Res.* **1,** 724 (1986).
13. A. T. Motta, D. R. Olander and A. J. Machiels, *Proc. 14th ASTM Symp. on the Effects of Irradiation on Materials*, ASTM STP 1046, pp. 451–469. Andover, Mass. (1988).
14. A. T. Motta, *Ph.D.thesis*, Univ. Calif. Berkeley (1988).
15. D. E. Luzzi, H. Mori and H. Fujita, *Scripta metall.* **19,** 897 (1985).
16. F. Garner, L. E. Thomas and D. S. Gelles, *CONF-750947, Proc. ASTM Symp. Exp. Methods for Charged-Particle Irradiations*, pp. 51–81. Gatlinburg. Tenn. (1975).
17. H. Mori, H. Fujita, M. Tendo and M. Fujita, *Scripta metall.* **18,** 783 (1984).
18. W. J. S. Yang, *Precipitate Stability in Zircaloy-4*, EPRI NP-5591 (1988).
19. F. Lefebvre and C. Lemaignan, *J. Nucl. Mater.* **165,** 122 (1989).
20. H. M. Chung, *Second Int. Symp. on Environmental Degradation of Materials in Nuclear Power Systems.* Monterey, Calif. (1985).
21. M. Griffiths, *J. Nucl. Mater.* **159,** 190 (1988).
22. M. P. Henaff, C. Colinet, A Pasturel and K. H. J. Buschow, *J. appl. Phys.* **56,** 307 (1984).
23. Z. Altounian, Tu Guo-hua and J. O. Strom-Olsen, *J. appl. Phys.* **54,** 3111 (1983).
24. N. Yoshida and M. Kiritani *J. Phys. Soc. Japan* **35,** 1418 (1973).
25. S. J. Rothman, N. Q. Lam, R. Sizmann and H. Bisswanger, *Radiat. Effects* **20,** 223(1973).
26. P. Gordon, *Principles of Phase Diagrams*, Chap. 4. McGraw–Hill, New York (1968).
27. S. Banerjee and K. Urban, *Physica status solidii (a)* **81,** 145 (1984).
28. M. A. Kirk and T. H. Blewitt, *Metall. Trans.* **9A,** 1729 (1978).
29. L. R. Aronin, *J. appl. Phys.* **25,** 344 (1954).
30. G. Hood, *J. Nucl. Mater.* **159,** 149 (1988).
31. J. Linnros, R. G. Elliman and W. L. Brown, *J. Mater. Res.* **3,** 1208 (1988).
32. L. L. Harris and W. J. S. Yang, *13th ASTM Symp. on the Effects of Irradiation on Materials*, Seattle, Wash. (1986).
33. M. L. Swanson, J. R. Parsons and C. W. Hoelke, *Radiat. Effects* **9,** 249 (1971).
34. K. Y. Liou and P. Wilkes, *J. Nucl. Mater.* **87,** 317 (1979).
35. G. J. Dienes, *Acta metall.* **3,** 549 (1955).
36. G. H. Vineyard, *Phys. Rev.* **102,** 981 (1956).
37. R. Zee and P. Wilkes, *Phil. Mag. A* **42,** 463 (1980).
38. M. Fuse, *J. Nucl. Mater.* **136,** 250 (1985).
39. P. Moser, private communication.

APPENDIX

Evaluation of Thermal Reordering

(1) Vacancy thermal Reordering

The motion of vacancies can reorder the lattice through the mechanism shown in Fig. 7(a) [35–37]. Vacancy motion can also disorder the lattice by jumping to the "wrong" site as in Fig. 7(b). Vacancy thermal reordering is then the net result of forward and backward reactions

$$A_b + A_{vac} \rightleftarrows A_a + B_{vac} \tag{A1}$$

where A_b is an A atom on a B site and A_{vac} is a vacancy on an A site. If we consider only nearest-neighbor jumps, the rate of the change in F_{aa} due to the forward reaction is

$$\left(\frac{dF_{aa}}{dt}\right)_{ord} = P_a J_v \tag{A2}$$

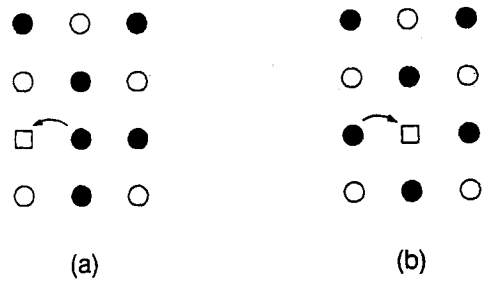

Fig. 7. Vacancy thermal reordering mechanisms: a reordering jump is shown in (a) and a disordering jump in (b).

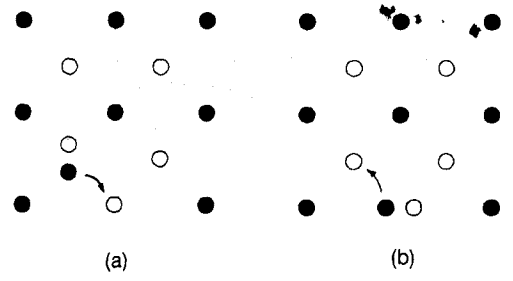

Fig. 8. Split-interstitial thermal reordering mechanism. The interstitial jumps shown in (a) and (b) correspond respectively to the forward and backward reactions in equation (A5) and have their favorable configurations listed in reaction 1 in Table 2.

where P_a is the fraction of sites that have a favorable configuration for the ordering jump to occur and J_v is the ordering jump frequency. The favorable configuration for the forward jump is an A vacancy nearest neighbor to an A atom in a B site so

$$P_a = C_{av}[1-(1-F_{bb})^{Z_{ba}}] \approx C_{av} F_{ab} Z_{ab} \qquad \text{(A3)}$$

where $C_{av} = x_a C_v$ is the A vacancy fraction and the Z_{ij} and F_{ij} are defined in Section 3.2.

The existence of a bias towards the ordering jumps is predicated on the existence of some degree of order in the system. As S decreases, the differentiation between A and B site decreases and eventually vanishes. This is taken into account by writing $V = V_0 S$ [35, 36]. From equations (A2), (A3) and (14), then

$$\begin{aligned}\left(\frac{dS}{dt}\right)_{Vac} &= v\,[e^{-(E_v - V)/k_B T} C_{av} F_{ab} Z_{ba} \\ &\quad - e^{-E_v/k_B T} C_{bv} F_{aa} Z_{ab}] \\ &= v C_v e^{-E_v/k_B T}\left[e^{V_0 S/k_B T}(1-S) Z_{ba}\frac{x_a}{x_b} \right. \\ &\quad \left. -\left(1+\frac{x_b}{x_a}S\right) Z_{ab}\right] \qquad \text{(A4)}\end{aligned}$$

here v is the vibration frequency (s^{-1}) and E_v is the energy barrier for the vacancy disordering jump. For an equiatomic alloy this expression reduces to Vineyard's [36].

The bracketed term in equation (A4) is of the order of 10 if $V \leqslant 0.1\,eV$. With $v = 10^{13}\,(s^{-1})$, $E_v = 1\,eV$, $C_v = 10^{-3}$ and $T = 300$ K, the value of $(dS/dt)_{Vac}$ is 10^{-6}, which is negligible compared to the random recombination disordering contribution given in Section 3.2.

(2) *Split-interstitial reordering*

The mechanism for split-interstitial reordering is shown in Fig. 8. As the interstitial atom moves through the lattice, reordering occurs by exchanging sites with atoms that were on "wrong" sites. Depending on the crystal structure and on the number of nearest neighbors, there are several possible jumps like the one above, which have different effects on the state of order of the system.

The specific reaction shown in Fig. 8(a) and 8(b) when written as a chemical reaction has the form

$$(B^i + A^i)^b + B^a \rightleftarrows B^b + (B^i + A^i)^a \qquad \text{(A5)}$$

where A and B are A and B atoms, and the superscripts a and b designate the A and B sublattices respectively. The superscript i means that the atom in question is associated with a lattice site as part of a split-interstitial configuration at that site. The reaction above is an ordering reaction because its net effect is to substitute an A atom on a B site for a B atom on a B site. This neglects the interstitials' contribution to the state of order of the system. However, at any one time there are about 10^{-10} atom fraction interstitials in the lattice. We can therefore neglect their contribution to the calculation of S, except as a means of rearranging the atoms in the lattice.

Following the same procedure as above, all the other possible split-interstitial jumps can be written as chemical reactions. Some of them are ordering-disordering reactions, and some have no effect.

Eliminating neutral reactions, there remain eight reactions that can affect S. Their rate of occurrence is given by the product of the number of favorable configurations and the jump frequency. For the forward reaction in equation (A5), for example, the number of favorable configurations is $F_{bb} F_{ab} Z_{ab} F_{ba}$.

The jump frequency is higher for the ordering jumps, since the migration energy is decreased by a small amount corresponding to the ordering energy V. If the number of favorable configurations is equivalent for all types of jumps, a net reordering effect is produced.

The reactions that influence S are listed in Table 2 with their respective number of favorable configurations. They are arranged so that the forward reaction is ordering. The reaction in equation (A5) is reaction (1) in Table 2.

If all ordering jumps have the same barrier, the jump rate is given by

$$J_{si} = v\, C_{si}\, e^{-E_{si}/k_B T} \qquad \text{(A6)}$$

Table 2. Reactions affecting the long-range order parameter S. Number of favorable configurations

	Reactions	Forward reaction	Reverse reaction
1	$(B^i + A^i)^b + B^a \rightleftarrows B^b + (B^i + A^i)^a$	$F_{bb}F_{ab}Z_{ab}F_{ba}$	$F_{ba}F_{aa}Z_{ba}F_{bb}$
2	$(B^i + A^i)^a + A^b \rightleftarrows A^a + (B^i + A^i)^b$	$F_{ba}F_{aa}Z_{ab}F_{ab}$	$F_{ab}F_{bb}Z_{ba}F_{aa}$
3	$(B^i + B^i)^b + B^a \rightleftarrows B^b + (B^i + B^i)^a$	$F_{bb}F_{bb}Z_{ba}F_{ba}$	$F_{ba}F_{ba}Z_{ab}F_{bb}$
4	$(A^i + A^i)^a + A^b \rightleftarrows A^a + (A^i + A^i)^b$	$F_{aa}F_{aa}Z_{ba}F_{ab}$	$F_{ab}F_{ab}Z_{ab}F_{aa}$
5	$(B^i + B^i)^b + A^b \rightleftarrows B^b + (B^i + A^i)^b$	$F_{bb}F_{bb}Z_{bb}F_{ab}$	$F_{bb}F_{ab}Z_{bb}F_{bb}$
6	$(B^i + A^i)^b + A^b \rightleftarrows B^b + (A^i + A^i)^b$	$F_{bb}F_{ab}Z_{bb}F_{ab}$	$F_{ab}F_{ab}Z_{bb}F_{bb}$
7	$(B^i + A^i)^a + B^a \rightleftarrows A^a + (B^i + B^i)^a$	$F_{ba}F_{aa}Z_{aa}F_{ba}$	$F_{ba}F_{ba}Z_{aa}F_{aa}$
8	$(A^i + A^i)^a + B^a \rightleftarrows A^a + (B^i + A^i)^a$	$F_{aa}F_{aa}Z_{aa}F_{ba}$	$F_{ba}F_{aa}Z_{aa}F_{aa}$

where C_{si} is the concentration of interstitials in the configuration shown in Fig. 8 and E_{si} is the migration energy for the split-interstitial jump. Since there are several possible interstial configurations [38], C_{si} is smaller than the total interstitial concentration C_i. The product of the jump rate and the number of favorable configurations gives the rate of variation in S

$$\begin{aligned}\left(\frac{dS}{dt}\right)_{si} = v\, C_{si}\, e^{-E_{si}/k_B T} [&Z_{ab}[(F_{ba}F_{ab}F_{bb} + F_{aa}F_{ab}F_{ba})e^{V_0 S/k_B T} \\ &- (F_{ba}^2 F_{bb} + F_{aa}F_{ab}^2)] \\ &+ Z_{ba}[(F_{bb}^2 F_{ba} + F_{aa}^2 F_{ab})e^{V_0 S/k_B T} \\ &- (F_{aa}F_{ba}F_{bb} + F_{aa}F_{bb}F_{ab})] \\ &+ Z_{aa}[(F_{aa}F_{ba}^2 + F_{ba}F_{aa}^2)(e^{V_0 S/k_B T} - 1)] \\ &+ Z_{bb}[(F_{bb}F_{ab}^2 + F_{ab}F_{bb}^2)(e^{V_0 S/k_B T} - 1). \qquad \text{(A7)}\end{aligned}$$

It is not possible to integrate directly eqn.(A7), so in order to compare the split-interstitial reordering term with the random recombination disordering term, an evaluation will be made of both for typical values. For $S = 0.5$, and $k = 10^{-3}$ dpa/s is the random recombination term [eqn.(17)] is equal to $5 \times 10^{-4}\,s^{-1}$. If $v = 10^{13}\ s^{-1}$, $C_{si} = 10^{-10}$, $T = 300\,K$, E_{si} should be 0.4 eV in order for the split-interstitial reordering term to have the same value. There is very little information on interstitial migration in concentrated alloys, but 0.4 eV is not an unreasonable value for the interstitial migration energy [39].

Therefore it is concluded that, in compounds where this migration mechanism is active, the split-interstitial reordering term can be of the same order of magnitude as the random recombination disordering term. It should be noted that the existence of split-interstitial migration only implies reordering if there is atom exchange between the two sublattices. If there is no exchange, the atom jumps occur within the individual sublattices and have no effect in the degree of order.